ZnO/g-C₃N₄ Nanostructured Photocatalyst for Enhancement of Photodegradation of Antibiotic Pollutant in Wastewater under Simulated solar Light Illumination

Nianping Chi[1,], Xinyi Yuan[1], Wen Sun[2]*

[1] School of Municipal and Geomatics Engineering, Hunan City University, Hunan Province Engineering & Technology Research Center for Rural Water Quality Safety, Yiyang, Hunan 413000, China
[2] School of Environmental Science and Engineering, Suzhou University of Science and Technology, Suzhou 215009, China
[*]E-mail: cnp2022zjgsdx@163.com

The fabrication and characterization of a ZnO/g-C₃N₄ nanostructured photocatalyst for improving photodegradation of tetracycline hydrochloride (TC-HCl) as an antibiotic pollutant in wastewater under simulated solar light were given in this study. The ZnO/g-C₃N₄ nanostructure was synthesized using the deposition–precipitation method, and the morphology and structure of the photocatalyst revealed that the hybrid structure was composed of well-crystalline ZnO nanostructures and homogeneously dispersed g-C₃N₄ nanosheets, implying a homogeneous and strong interaction of g-C₃N₄ with ZnO nanostructures. The optical band gap values of g-C₃N₄, ZnO, and ZnO/g-C₃N₄ hybrid structures were calculated to be 2.70, 3.16, and 2.90 eV, respectively, based on the optical properties. Electrochemical experiments revealed that the ZnO/g-C₃N₄ hybrid structure has a higher interfacial charge transfer efficiency, less recombination of photogenerated electron–hole pairs, and enhanced electron mobility and diffusion. Using g-C₃N₄, ZnO, and ZnO/g-C₃N₄ hybrid structures, 88%, 65%, and 100% degradation efficiencies were obtained for treatment of 200 mL of 10 mg/L of TC-HCl aqueous solution after 45 minutes of simulated solar light illumination, respectively, implying that the ZnO/g-C₃N₄ heterojunction can remarkably improve solar light photocatalytic activity. Finally, the data showed that ZnO/g-C₃N₄ hybrid photodegradation was effective in treating TC-HCl from real pharmaceutical industrial effluent.

Keywords: Photocatalyst; Antibiotic pollutant; ZnO/g-C₃N₄; Tetracycline hydrochloride; Pharmaceutical industry wastewater

1. INTRODUCTION

Antibiotics are among the most effective medications in human medicine [1]. They must, nevertheless, be regarded as important pollutants since they can pose a threat to microbial communities [2, 3]. Antibiotics are increasingly being used for animal farming and agricultural purposes, in addition to human medicine. Antibiotics that have been used are discarded or flushed down drains or toilets [4, 5]. Antibiotics in manure and other waste-based fertilizers wash off into waterways from agriculture and pasture fields. Our pets' feces carrying antibiotics winds up in landfills and neighborhood sewer runoff.

Antibiotics given to humans and animals are eliminated in their natural state in feces and urine [6, 7]. The manure is high in nutrients and is frequently utilized as a fertilizer on crop fields, resulting in direct contamination of the environment with antibiotic residues and resistant microorganisms. Drug-resistant bacteria that have developed new resistance mechanisms, leading to antimicrobial resistance, continue to pose a danger to our capacity to treat common diseases [8, 9].

Tetracycline Hydrochloride (TC-HCl, $C_{22}H_{24}N_2O_8.HCl$) is a broad-spectrum naphthacene antibiotic synthesized semisynthetically from chlortetracycline, an antibiotic obtained from the bacteria Streptomyces aureofaciens [10, 11]. TC-HCl is an antibiotic that is used to treat a range of illnesses, including acne [12, 13]. It's an antibiotic that works by preventing germs from growing. Only bacterial infections of the testes, plague, bacterial infections caused by deer fly, flea, and tick bites, an infection of the female reproductive systems known as pelvic inflammatory disease, and infections of the skin and tissue beneath the skin are treated with this antibiotic [14]. Discoloration of teeth and enamel hypoplasia are common adverse effects of TC-HCl, as are diarrhea, nausea, photosensitivity, stomach distress, lack of appetite, white patches or ulcers within mouth or on lips, and swollen tongue [15-17]. Because TC-HCl is difficult to metabolize in the human and animal digestive systems, it is expelled into the environment up to 50%−80% via human feces and animal excreta [10, 18]. Moreover, hospitals, pharmaceutical industries, and livestock also contribute to the cumulative accumulation of TC-HCl in the wastewater systems.

Therefore, degradation of antibiotics is important and many studies have been conducted for the treatment of antibiotic pollutants in wastewater [19-27]. Hydrolysis, chemical oxidation, photolysis, biodegradation, desorption, adsorption and photocatalysis are generally considered the important pathways for degradation of antibiotics [19, 28]. Many of these degradation methods cause to the chemical bonds to break or decompose, and produce a large amount of secondary pollution [29, 30]. Photocatalysis is an environmentally benign and low-cost process that has tremendous potential as an effective and sustainable oxidation technology for wastewater treatment and antimicrobial pollutant reduction in wastewater when exposed to light. As a result, this research focused on the synthesis and characterization of a $ZnO/g-C_3N_4$ photocatalyst for improved photodegradation of TC-HCl as an antibiotic pollutant in wastewater under simulated solar light illumination.

2. EXPERIMENT

2.1. Synthesis of ZnO/g-C₃N₄ photocatalyst

The following process [31] was used to synthesize the ZnO/g-C$_3$N$_4$ photocatalyst at room temperature using the deposition–precipitation method: In 30 mL of 0.5 M ZnCl$_2$ (96%, Hainan Yanghang Industrial Co., Ltd., China) solution, 0.08 g of melamine (99%, Sigma-Aldrich) was added, and the mixture was magnetically agitated for 30 minutes. After that, 30 mL of 0.5 M Na$_2$CO$_3$ (99.5%, Sigma-Aldrich) solution was slowly added to the mixture, which was then agitated for another 25 minutes. To obtain ZnO/g-C$_3$N$_4$ photocatalyst, the agitated mixture was filtered over a black grid Millipore membrane (0.45 μm Millipore Corp., Bedford, Mass), washed three times with deionized water, and dried at 75°C for 20 hours. The preparation of g-C$_3$N$_4$ was carried out in this manner without adding ZnCl$_2$, and ZnO photocatalyst was also synthesized using the same procedure without adding melamine.

2.2. Photodegradation measurements

All photodegradation tests were done in a batch reactor with a cylindrical Pyrex-glass cell that was irradiated from above using a solar simulator (Newport, USA) equipped with a 450 W Xenon arc lamp (Wenzhou Bozhou Marine Electrical Co., Ltd., China). The lamp was placed in the reactor's middle, with an 8-cm distance between it and the solution inside. 200 mL of TC-HCl aqueous solution (5, 10, 20, and 50 mg/L concentrations) and 1 g/L photocatalysts (g-C$_3$N$_4$, ZnO, and ZnO/g-C$_3$N$_4$) powders were added to the photoreactor. The mixes were agitated with a magnetic stirrer to keep them consistent. Prior to photodegradation measurements, the mixtures were magnetically stirred under dark conditions for 40 minutes to reach the adsorption-desorption equilibrium between the TC-HCl molecules and photocatalyst particles. After irradiation with light, the suspensions were collected and filtered through Millipore membrane to remove any photocatalyst particles. Then, the concentration of TC-HCl was measured via a spectrophotometer (UV-2550, Shimadzu, Kyoto, Japan) at 357 nm [32, 33]. The degradation efficiency of TC-HCl is calculated by [34, 35]:

$$\text{Degradation efficiency (\%)} = \frac{C_0 - C_t}{C_0} \times 100 \qquad (1)$$

Where C_0 is initial concentration of the TC-HCl and C_t is concentration of the TC-HCl after photo-irradiation.

2.3. Instruments and characterizations

The shape and structure of photocatalysts were studied using scanning electron microscopy (SEM; Zeiss Ultra Plus, Germany) and X-ray diffraction (XRD; Bruker D8 127, D8 advance, USA). Aspectrum of UV–Vis absorption was acquired using a UV–Visible spectrophotometer (UV-2550, Shimadzu, Kyoto, Japan). An electrochemical impedance spectroscopy (EIS) analysis was applied to a working electrode (photocatalysts modified Indium tin oxide (ITO) coated glass), a counter electrode (Pt foil), and a reference electrode (Ag/AgCl) using an electrochemical setup (CHI 660E, USA). EIS

studies were conducted in a 0.5 M Na_2SO_4 (99%, Merck, Germany) solution over a frequency range of 10^{-1}–10^5 Hz with a 10 mV amplitude.

3. RESULTS AND DISCUSSION

3.1. Study of morphology and structure of photocatalysts

The SEM picture of g-C_3N_4, ZnO, and ZnO/g-C_3N_4 hybrid structures is shown in Figure 1. The surface morphology of pure g-C3N4 nanostructure has a nanosheet-like and fluffy structure, as shown in Figure 1a. Figure 1b displays a SEM image of pure ZnO with nanorod-shaped nanoparticles corresponding to the hexagonal crystallographic plane (0001) of ZnO with an average diameter of 70. The SEM image of the ZnO/g-C_3N_4 hybrid structure in Figure 1c shows that the hybrid structure is made up of ZnO nanostructures and g-C3N4 nanosheets that are evenly spread, implying a homogenous and strong contact between g-C_3N_4 and ZnO nanostructures. There is a high porosity surface where ZnO nanostructures are wrapped with g-C_3N_4 which is believed to be critical for the efficient formation of heterojunction and favorable for the photocatalyst to absorb pollutants and further promote the degradation ability of the ZnO/g-C_3N_4 hybrid structure [36-38].
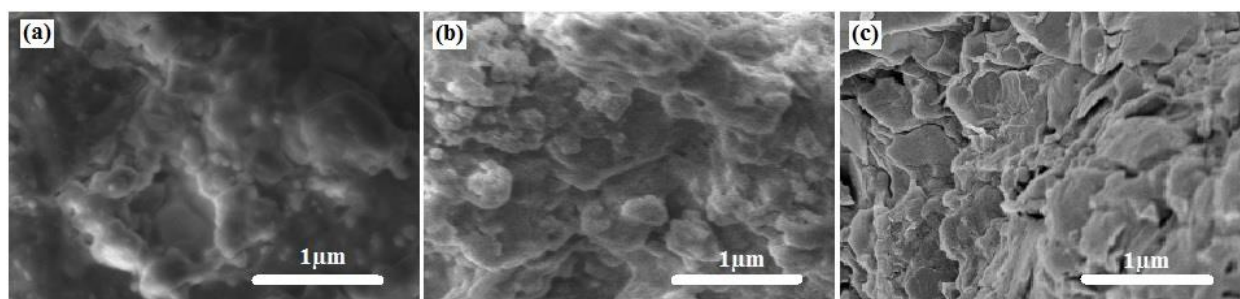

Figure 1. SEM image of (a) g-C3N4, (b) ZnO and (c) ZnO/g-C3N4 hybrid structures.
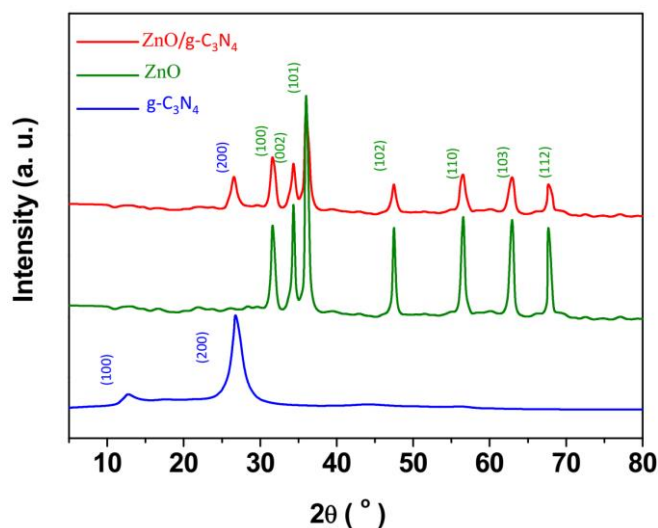

Figure 2. XRD patterns of powders of g-C_3N_4, ZnO and ZnO/g-C_3N_4 hybrid structures.

Figure 2 shows XRD patterns of powders of g-C$_3$N$_4$, ZnO, and ZnO/g-C$_3$N$_4$ hybrid structures. The in-plane structure of tris-triazine units and the inter-planar stacking of -conjugated aromatic systems of g-C$_3$N$_4$ are related to the in-plane structure of tris-triazine units and the inter-planar stacking of -conjugated aromatic systems of g-C$_3$N$_4$ respectively [39-41]. XRD patterns of ZnO and ZnO/g-C$_3$N$_4$ hybrid structures show diffraction peaks at 2θ = 31.65°, 34.21°, 36.03°, 47.51°, 56.30°, 63.11°, and 67.59°, which correspond to the hexagonal wurtzite structure of ZnO and are indexed as the (100), (002), (101), (102), (110), (103), and (112) planes (JCPDS card no. 36-1451) [42, 43]. XRD patterns of ZnO/g-C$_3$N$_4$ hybrid structure displays shows the additional diffraction peak of (002) plane of g-C$_3$N$_4$, demonstrating successfully synthesized ZnO/g-C$_3$N$_4$ hybrid by deposition–precipitation method.

3.2. Optical properties of photocatalysts

Figure 3a shows the UV–vis absorption spectra of g-C3N4, ZnO, and ZnO/g-C$_3$N$_4$ hybrid structures. As can be seen, the light absorption intensity of g-C3N4 toward ZnO increases dramatically in the UV and visible ranges. This is due to the 2D planar structure of the –conjugated (–CN) g-C$_3$N$_4$ matrix, which benefits charge carrier movement [44-46]. The optical absorbance spectra of ZnO show a remarkable sharp absorption edge in the UV region and low absorption in the visible light region, which is attributed to pure ZnO's intrinsic band-gap energy and sensitivity to UV light [47, 48]. Optical absorbance spectra of the ZnO/g-C$_3$N$_4$ hybrid show a red shift in absorption compared to pure ZnO. The light absorption intensity of ZnO/g-C$_3$N$_4$ toward ZnO is also increased in UV and visible regions. It is associated with the fact that g-C$_3$N$_4$ is the conductive polymer and the addition of g-C$_3$N$_4$ in the ZnO structure generates the intermediate energy level which improves the light absorption ability in both of UV and visible regions [49, 50]. The band gap energy (Eg) value for samples can be estimated using the following equation [51]:

$$(\alpha h\nu)^{1/2} = A(h\nu - Eg) \qquad (2)$$

Where α and $h\nu$ are the absorption coefficient and the photon energy, respectively, and A is the proportionality parameter. The Eg values of g-C$_3$N$_4$, ZnOand ZnO/g-C$_3$N$_4$ hybrid structures were determined by plotting Tauc's plots using intercepts of the extrapolating the straight-line part plots between $(\alpha h\nu)^{1/2}$ versus photon-energy ($h\nu$) as exhibited in Figure 3b. Eg values for g-C$_3$N$_4$, ZnO, and ZnO/g-C$_3$N$_4$ hybrid structures were discovered to be 2.70, 3.16, and 2.90 eV, respectively. It is shown that the optical band gap of ZnO/g-C$_3$N$_4$ hybrid structure decreases toward ZnO due to the introduction of g-C$_3$N$_4$, and formation of heterojunction structure between ZnO with a wide band gap energy and g-C$_3$N$_4$ with a narrow band gap energy [52-54]. Because g-C$_3$N$_4$ has a higher electrical conductivity than ZnO, it enhances electron density in heterojunction structures and creates new intermediate energy levels between the valence and conduction bands, resulting in quick charge transfer and separation between the two materials [55, 56], and leads to enhanced photocatalytic activity of ZnO/g-C$_3$N$_4$ hybrid structures under visible light irradiation.
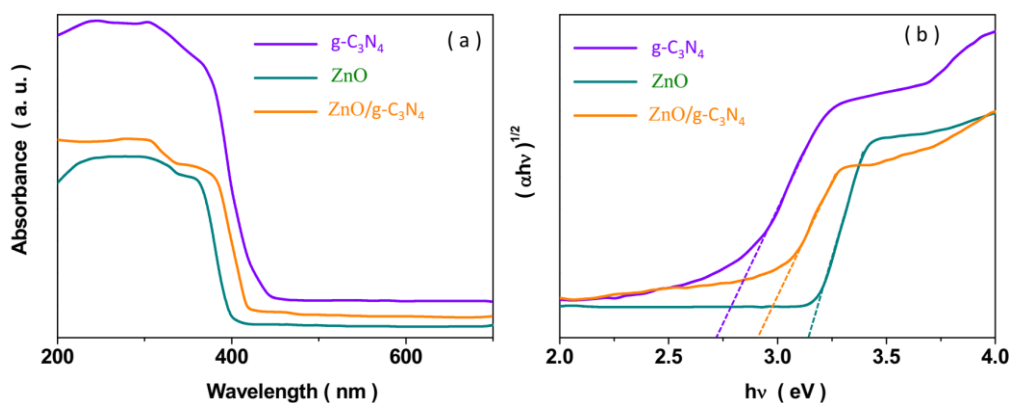
Figure 3. (a) UV–vis absorption spectra and (b) related Tauc plots of g-C_3N_4, ZnO and ZnO/g-C_3N_4 hybrid structures

Figures 4a and 4b show the Nyquist and bode plots for g-C_3N_4, ZnO and ZnO/g-C_3N_4 hybrid structures under light illumination, respectively. As seen, the Nyquist plots show two semicircles; the the smaller semicircle is related to the higher frequency region (10^3–10^5 Hz) and the predominant semicircle corresponds to the medium frequency region (10^{-1}–10^3 Hz). Figure 4a shows an equivalent electrical circuit model with two parallel resistors (R) and constant-phase-elements (C) coupled in a series resistor. The characteristics acquired from the equivalent circuit are provided in Table 1. (Rs). The ohmic resistance of an electrolyte is measured in Rs.
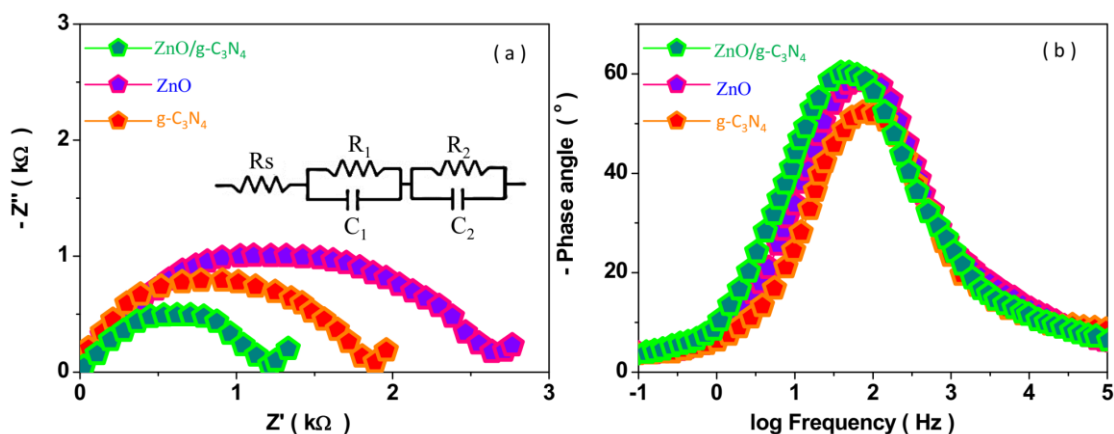

Figure 4. (a) The Nyquist and the equivalent circuit, and (b) bode plots for g-C_3N_4, ZnO and ZnO/g-C_3N_4 hybrid structures under light illumination.

The high-frequency semicircle is represented by C1, which stands for double layer capacitance, and R1, which stands for carrier transport resistance in the bulk. The dominating semicircle is linked to C2 and R2, implying carrier transport activities at the photocatalyst/electrolyte interface [57-59]. Charge-transfer and recombination activities at the electrode/electrolyte interface are reflected in the higher frequency region semicircle, and the semicircle diameters in Nyquist diagrams reveal charge-

transfer kinetics at the electrode interface. The ZnO/g-C$_3$N$_4$ hybrid has the smallest semicircle, indicating improved interfacial charge transfer efficiency, less recombination of photogenerated electron–hole pairs, and greater electron mobility and diffusion [60, 61]. The lifetime (τ) of the photogenerated electrons can be estimated using the maximum peak frequency (f_{max}) in bode plots according to $\tau_n = 1/(2\pi f_{max})$, which indicates that the lifetime is inversely proportional to the peak frequency [62]. As seen from Table 1, the calculated electron lifetimes of the ZnO/g-C$_3$N$_4$ hybrid are the longest as indicated by its largest separation efficiency [63].

Table 1. The parameters obtained from the equivalent circuit.

Sample	R$_1$ (Ω)	C$_1$ (μF)	R$_1$ (Ω)	C$_2$ (μF)	τ (ms)
g-C$_3$N$_4$	33.8	22.4	15.59	19.5	4.1
ZnO	41.1	23.5	12.22	14.9	3.1
ZnO/g-C$_3$N$_4$	29.7	17.5	6.09	15.2	2.2

3.4. Evaluation the photocatalytic performance

To assess the photocatalytic performance of g-C$_3$N$_4$, ZnO, and ZnO/g-C$_3$N$_4$ hybrid structures for the treatment of TC-HCl, photodegradation measurements were carried out in 200 mL of 10 mg/L of TC-HCl aqueous solution under simulated solar light illumination in three conditions with a photocatalyst of g-C$_3$N$_4$, ZnO, and ZnO/g-C$_3$N$_4$ hybrid structures (Figure 5). Figure 5 demonstrates that after 90 minutes of simulated solar light irradiation, the control sample has an 8% degradation efficiency, indicating that the TC-HCl molecule is very stable and cannot be degraded without the use of a photocatalyst [64, 65]. As observed, 88%, 65% and 100% degradation efficiencies belong to g-C$_3$N$_4$, ZnO and ZnO/g-C$_3$N$_4$ hybrid structures after 45 minutes of simulated solar light, respectively. Structures with 100% degradation of TC-HCl are obtained after 65 and 90 minutes of simulated solar light for g-C$_3$N$_4$ and ZnO, respectively. ZnO has the worst photodegradation performance due to its greater band gap, which cannot be initiated by simulated solar light illumination. Because g-C$_3$N$_4$ has a higher electrical conductivity than the hybrid structure, it has a lower photocatalytic activity. This is due to the higher absorption ability of irradiated photon energy by electrons in the conduction band. The ZnO/g-C$_3$N$_4$ hybrid structure, on the other hand, exhibits the maximum TC-HCl degradation, implying that the ZnO/g-C$_3$N$_4$ heterojunction can significantly boost solar light photocatalytic activity [66, 67]. The synergetic effect of ZnO and g-C$_3$N$_4$ promotes the formation of hetero-junction structures and generates a novel and highly efficient photocatalyst as suggested by the following mechanism [49]. When ZnO/g-C$_3$N$_4$ heterojunction is irradiated under simulated solar light, the electrons of ZnO/g-C$_3$N$_4$ can be excited from the highest occupied molecular orbital (HOMO) to the lowest unoccupied molecular orbital (LUMO) level of g-C$_3$N$_4$, subsequently, the photogenerated electrons can be injected to the conduction band of ZnO. Therefore, photo-generated holes will be left in the HOMO levels of g-C$_3$N$_4$ due to the LUMO level of g-C$_3$N$_4$ (-1.1 eV vs. Normal Hydrogen Electrode, NHE) is more negative than the conduction band edge of ZnO (-0.27 eV vs. NHE) [49]. The electrons in

valence band of ZnO can transfer to the HOMO of g-C$_3$N$_4$ to recombine with holes. Simultaneously, the holes photogenerate in the valence band of ZnO. Consequently, the lifetime of photogenerated electrons and holes is increased, and more and more photogenerated carriers form in the ZnO nanostructure. The photogenerated electrons can react with O$_2$ to form superoxide radical (O$^{\bullet-}_2$), at the same time, the photogenerated holes can react with OH$^-$ or H$_2$O to create a hydroxyl radical (•OH) [68, 69]. These radicals can react with TC-HCl molecules. Thus, the findings illustrate that ZnO/g-C$_3$N$_4$ heterojunction can be utilized as promising candidate for application in the treatment of antibiotic pollutants and environmental purification.
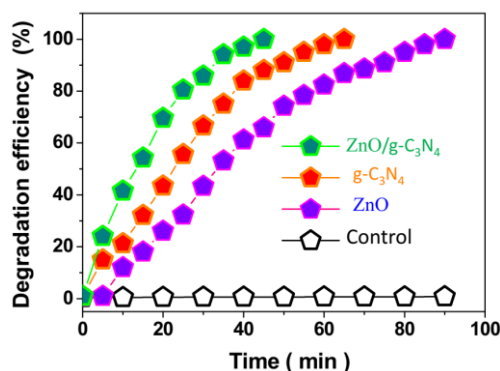

Figure 5. Photodegradation efficiency of g-C$_3$N$_4$, ZnO and ZnO/g-C$_3$N$_4$ hybrid structures for treatment 200 mL of 10 mg/L of TC-HCl aqueous solution upon simulated solar light illumination.
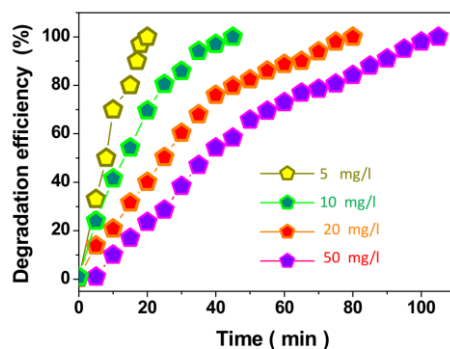

Figure 5. Photodegradation efficiency of ZnO/g-C$_3$N$_4$ hybrid structure for treatment 200 mL of 5, 10, 20 and 50 mg/L of TC-HCl aqueous solution upon simulated solar light illumination.

The photodegradation efficiency of ZnO/g-C$_3$N$_4$ hybrid for treatment of 200 mL of TC-HCl aqueous solution with different intimal concentrations was investigated upon simulated solar light illumination. Figure 6 demonstrates that photocatalytic degradation efficiency decreases with increasing initial TC-HCl concentration. The total degradation of 5, 10, 20 and 50 mg/L of TC-HCl is obtained after 20, 45, 80, and 105 minutes of simulated solar light illumination, respectively. These findings were compared with the reported photodegradation efficiency of various published photocatalysts for the treatment of TC-HCl which presented in Table 2. As observed from Table 2, the

ZnO/g-C$_3$N$_4$ hybrid shows a high photocatalytic efficiency that originates from its efficient separation of electron–hole pairs [66].

Table 1. Comparison of between the photodegradation efficiency ZnO/g-C$_3$N$_4$ hybrid and reported various published photocatalysts for the treatment of TC-HCl.

Catalyst	Amount of TC-HCl (mg/L)	Light source	Degradation efficiency (%)	Degradation time (minute)	Ref.
C–N–S tridoped TiO$_2$	5	Visible	97	180	[26]
MWCNT/TiO$_2$	10	UV	83	300	[20]
TiO$_2$-P25	10	UV	94.8	120	[21]
TiO$_2$-P25	20	UV	100	75	[22]
Fe-based metal–organic frameworks	50	Visible	96.6	180	[24]
TiO$_2$-P25	55	UV	100	120	[23]
ZnO/g-C$_3$N$_4$	5	solar	100	20	This work
	10			45	
	20			80	
	50			105	

3.5. Treatment of real pharmaceutical industry wastewater

The photodegradation ability of the ZnO/g-C$_3$N$_4$ hybrid was tested for treatment of 200 mL of 5 mg/L TC-HCl solution created from real pharmaceutical company wastewater (S1, China National Pharmaceutical Group Co., Ltd., Beijing, China), which was compared to a sample made with deionized wastewater (S2). Figure 7 shows the photodegradation of S1 and S2 after 45 and 20 minutes of treatment, respectively, under simulated solar-light. Because of the presence of various organic and intermediate metabolites in pharmaceutical industry effluent, a longer treatment time is necessary to completely degrade TC-HCl from an actual sample [20]. Meanwhile, the findings demonstrate the efficient photodegradation of the ZnO/g-C$_3$N$_4$ hybrid for treatment of TC-HCl from real pharmaceutical industry wastewater.
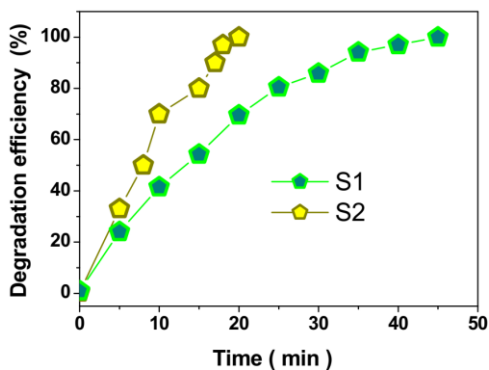

Figure 7. Photodegradation efficiency of ZnO/g-C$_3$N$_4$ hybrid for treatment the 200 mL of 5 mg/L TC-HCl solution made from real pharmaceutical industry wastewater (S1) and sample prepared with deionized wastewater (S2).

4. CONCLUSION

This research focused on the fabrication and characterization of a ZnO/g-C$_3$N$_4$ nanostructured photocatalyst for improving the photodegradation of TC-HCl as an antibiotic contaminant in wastewater under simulated solar light illumination. The ZnO/g-C$_3$N$_4$ nanostructure was synthesized using the deposition–precipitation method, and the morphology and structure of the photocatalyst revealed that the hybrid structure was composed of well-crystalline ZnO nanostructures and homogeneously dispersed g-C3N4 nanosheets, implying a homogeneous and strong interaction of g-C$_3$N$_4$ with ZnO nanostructures. Results of the optical properties showed that the optical band gap values of g-C$_3$N$_4$, ZnO and ZnO/g-C$_3$N$_4$ hybrid structures were estimated ~2.70, 3.16 and 2.90 eV, respectively, indicating the optical band gap of ZnO/g-C$_3$N$_4$ hybrid structure decreased toward ZnO due to the introduction of g-C$_3$N$_4$, and the formation of a heterojunction structure between ZnO with wide band gap energy and g-C$_3$N$_4$ with a narrow band gap energy which resulted in the fast charge transfer and separation between g-C$_3$N$_4$ and ZnO, and which resulted in the photocatalytic activity of ZnO/g-C$_3$N$_4$ hybrid structure under visible light irradiation. Electrochemical studies indicated greater interfacial charge transfer efficiency, the low recombination of photogenerated electron–hole pairs, and the greater mobility and diffusion of electrons in the ZnO/g-C$_3$N$_4$ hybrid structure. Using g-C3N4, ZnO, and ZnO/g-C$_3$N$_4$ hybrid structures, 88%, 65%, and 100% degradation efficiencies were obtained for treatment of 200 mL of 10 mg/L of TC-HCl aqueous solution after 45 minutes of simulated solar light illumination, respectively, implying that the ZnO/g-C$_3$N$_4$ heterojunction can remarkably improve solar light photocatalytic activity. Finally, the data showed that ZnO/g-C$_3$N$_4$ hybrid photodegradation was effective in treating TC-HCl from real pharmaceutical industrial effluent.

References

1. M. Bacanlı and N. Başaran, *Food and Chemical Toxicology*, 125 (2019) 462.
2. D. Xu, J. Liu, T. Ma, X. Zhao, H. Ma and J. Li, *Environmental Technology & Innovation*, 26 (2022) 102264.
3. H. Karimi-Maleh, H. Beitollahi, P.S. Kumar, S. Tajik, P.M. Jahani, F. Karimi, C. Karaman, Y. Vasseghian, M. Baghayeri and J. Rouhi, *Food and Chemical Toxicology*, (2022) 112961.
4. D. Cheng, H.H. Ngo, W. Guo, S.W. Chang, D.D. Nguyen, Y. Liu, Q. Wei and D. Wei, *Journal of hazardous materials*, 387 (2020) 121682.
5. U. Saindane, S. Soni and J. Menghani, *International Journal of Engineering*, 34 (2021) 2517.
6. L. Xu, H. Zhang, P. Xiong, Q. Zhu, C. Liao and G. Jiang, *Science of the Total Environment*, 753 (2021) 141975.
7. L. Zhang, Y. Xu, H. Liu, Y. Li, S. You, J. Zhao and J. Zhang, *Journal of Water Process Engineering*, 44 (2021) 102368.
8. F. Micoli, F. Bagnoli, R. Rappuoli and D. Serruto, *Nature Reviews Microbiology*, 19 (2021) 287.
9. W. Liu, F. Huang, Y. Liao, J. Zhang, G. Ren, Z. Zhuang, J. Zhen, Z. Lin and C. Wang, *Angewandte Chemie*, 120 (2008) 5701.

10.   A.A. Borghi and M.S.A. Palma, *Brazilian Journal of Pharmaceutical Sciences*, 50 (2014) 25.

11.   C. Shi, Z. Wu, F. Yang and Y. Tang, *Solid State Sciences*, 119 (2021) 106702.

12.   H. Liu, J. Yang, Y. Jia, Z. Wang, M. Jiang, K. Shen, H. Zhao, Y. Guo, Y. Guo and L. Wang, *Environmental Science & Technology*, 55 (2021) 10734.

13.   M. Khosravi, *European journal of translational myology*, 31 (2021) 9411.

14.   X. Tian, R. Yang, T. Chen, Y. Cao, H. Deng, M. Zhang and X. Jiang, *Journal of Hazardous Materials*, 426 (2022) 128121.

15.   B.M. SEGAL, *Archives of internal medicine*, 112 (1963) 165.

16.   M.-R. Wang, L. Deng, G.-C. Liu, L. Wen, J.-G. Wang, K.-B. Huang, H.-T. Tang and Y.-M. Pan, *Organic letters*, 21 (2019) 4929.

17.   M. Ghalandarzadeh and S. Afrang, *International Journal of Engineering*, 34 (2021) 2534.

18.   Y. Dai, M. Liu, J. Li, S. Yang, Y. Sun, Q. Sun, W. Wang, L. Lu, K. Zhang and J. Xu, *Separation Science and Technology*, 55 (2020) 1005.

19.   Q. Yang, Y. Gao, J. Ke, P.L. Show, Y. Ge, Y. Liu, R. Guo and J. Chen, *Bioengineered*, 12 (2021) 7376.

20.   L. Feng, X.H. Li, W.C. Lu, Z. Liu, C. Xu, Y. Chen, H.L. Zheng. *International Journal of Biological Macromolecules*, 150 (2020) 617.

21.   S. Wu, H. Hu, Y. Lin, J. Zhang and Y.H. Hu, *Chemical Engineering Journal*, 382 (2020) 122842.

22.   R.A. Palominos, M.A. Mondaca, A. Giraldo, G. Peñuela, M. Pérez-Moya and H.D. Mansilla, *Catalysis Today*, 144 (2009) 100.

23.   G.H. Safari, M. Hoseini, M. Seyedsalehi, H. Kamani, J. Jaafari and A.H. Mahvi, *International Journal of Environmental Science and Technology*, 12 (2015) 603.

24.   D. Wang, F. Jia, H. Wang, F. Chen, Y. Fang, W. Dong, G. Zeng, X. Li, Q. Yang and X. Yuan, *Journal of colloid and interface science*, 519 (2018) 273.

25.   L. Feng, J.J. Liu, Z.C. Guo, T.Y. Pan, J.H. Wu, X.H. Li, B.Z. Liu and H.L. Zheng, *Separation and Purification Technology*, 285 (2021)120314.

26.   P. Wang, P.-S. Yap and T.-T. Lim, *Applied Catalysis A: General*, 399 (2011) 252.

27.   H. Karimi-Maleh, C. Karaman, O. Karaman, F. Karimi, Y. Vasseghian, L. Fu, M. Baghayeri, J. Rouhi, P. Senthil Kumar and P.-L. Show, *Journal of Nanostructure in Chemistry*, (2022) 1.

28.   X. Lin, K. Lu, A.K. Hardison, Z. Liu, X. Xu, D. Gao, J. Gong and W.S. Gardner, *Ecological Indicators*, 126 (2021) 107639.

29.   Y. Zhang, J. Zhou, X. Chen, L. Wang and W. Cai, *Chemical Engineering Journal*, 369 (2019) 745.

30.   L. Zhang, L. Wang, Y. Zhang, D. Wang, J. Guo, M. Zhang and Y. Li, *Environmental research*, 206 (2022) 112629.

31.   W. Liu, M. Wang, C. Xu and S. Chen, *Chemical Engineering Journal*, 209 (2012) 386.

32.   C. Ma, J. Wei, K. Jiang, Z. Yang, X. Yang, K. Yang, Y. Zhang and C. Zhang, *Chemosphere*, 283 (2021) 131228.

33.   R. Rahmi, S. Lubis, N. Az-Zahra, K. Puspita and M. Iqhrammullah, *International Journal of Engineering*, 34 (2021) 1827.

34.   B. Han, R. Wang, X. Wei and R. Gu, *International Journal of Electrochemical Science*, 16 (2021) 210715.

35.   L. Yu and B. Tang, *International Journal of Electrochemical Science*, 16 (2021) 210915.

36.   X. Guo, J. Duan, C. Li, Z. Zhang and W. Wang, *Journal of Materials Science*, 55 (2020) 2018.

37.   R.C. Ngullie, S.O. Alaswad, K. Bhuvaneswari, P. Shanmugam, T. Pazhanivel and P. Arunachalam, *Coatings*, 10 (2020) 500.

38.   H. Li, Y. Zhang, C. Li, Z. Zhou, X. Nie, Y. Chen, H. Cao, B. Liu, N. Zhang and Z. Said, *Korean Journal of Chemical Engineering*, 39 (2022) 1107.

39. Á. Pérez-Molina, L.M. Pastrana-Martínez, L.T. Pérez-Poyatos, S. Morales-Torres and F.J. Maldonado-Hódar, *Nanomaterials*, 12 (2022) 340.

40. V. Shrivastava, I. Ali, M.M. Marjub, E.R. Rene and A.M.F. Soto, *Chemosphere*, 293 (2022) 133553.

41. H. Karimi-Maleh, R. Darabi, M. Shabani-Nooshabadi, M. Baghayeri, F. Karimi, J. Rouhi, M. Alizadeh, O. Karaman, Y. Vasseghian and C. Karaman, *Food and Chemical Toxicology*, 162 (2022) 112907.

42. J. Rouhi, H.K. Malayeri, S. Kakooei, R. Karimzadeh, S. Alrokayan, H. Khan and M.R. Mahmood, *International Journal of Electrochemical Science*, 13 (2018) 9742.

43. M. Khosravi, *Open Access Macedonian Journal of Medical Sciences*, 8 (2020) 553.

44. H. Li, X. Wu, S. Yin, K. Katsumata and Y. Wang, *Applied Surface Science*, 392 (2017) 531.

45. Ö. Tuna, E.B. Simsek, I. Dashan and G. Temel, *Journal of Photochemistry and Photobiology A: Chemistry*, 396 (2020) 112519.

46. R. Dalvand, S. Mahmud, J. Rouhi and C.R. Ooi, *Materials Letters*, 146 (2015) 65.

47. H.-L. Guo, Q. Zhu, X.-L. Wu, Y.-F. Jiang, X. Xie and A.-W. Xu, *Nanoscale*, 7 (2015) 7216.

48. J. Liu, Q. Zhang, X. Tian, Y. Hong, Y. Nie, N. Su, G. Jin, Z. Zhai and C. Fu, *Chemical Engineering Journal*, 404 (2021) 127146.

49. J.G.M. de Sousa, T.V.C. da Silva, N.P. de Moraes, M.L.C.P. da Silva, R. da Silva Rocha, R. Landers and L.A. Rodrigues, *Materials Chemistry and Physics*, 256 (2020) 123651.

50. L. Nan, C. Yalan, L. Jixiang, O. Dujuan, D. Wenhui, J. Rouhi and M. Mustapha, *RSC Advances*, 10 (2020) 27923.

51. Z. Wang, A. He and L. Liu, *International Journal of Electrochemical Science*, 17 (2022) 220645.

52. N. Kumaresan, M.M.A. Sinthiya, M.P. Kumar, S. Ravichandran, R.R. Babu, K. Sethurman and K. Ramamurthi, *Arabian Journal of Chemistry*, 13 (2020) 2826.

53. H. Li, Y. Zhang, C. Li, Z. Zhou, X. Nie, Y. Chen, H. Cao, B. Liu, N. Zhang and Z. Said, *The International Journal of Advanced Manufacturing Technology*, 120 (2022) 1.

54. E. Darezereshki, A. Behrad Vakylabad and M. Yousefi, *International Journal of Engineering*, 34 (2021) 1888.

55. M. Ismael, *Chemical Physics Letters*, 739 (2020) 136992.

56. H. Maleh, M. Alizadeh, F. Karimi, M. Baghayeri, L. Fu, J. Rouhi, C. Karaman, O. Karaman and R. Boukherroub, *Chemosphere*, (2021) 132928.

57. J. Park, I. Choi, M.J. Lee, M.H. Kim, T. Lim, K.H. Park, J. Jang, S.M. Oh, S.K. Cho and J.J. Kim, *Electrochimica Acta*, 132 (2014) 338.

58. D. Ge, H. Yuan, J. Xiao and N. Zhu, *Science of The Total Environment*, 679 (2019) 298.

59. C. Liu and J. Rouhi, *RSC Advances*, 11 (2021) 9933.

60. M.M. Islam, R.D. Tentu and S. Basu, *ChemistrySelect*, 3 (2018) 486.

61. T. Gao, Y. Zhang, C. Li, Y. Wang, Q. An, B. Liu, Z. Said and S. Sharma, *Scientific reports*, 11 (2021) 1.

62. O.V. Nkwachukwu, C. Muzenda, B.O. Ojo, B.N. Zwane, B.A. Koiki, B.O. Orimolade, D. Nkosi, N. Mabuba and O.A. Arotiba, *Catalysts*, 11 (2021) 1069.

63. X. Zhang, Y.-Z. Zhou, D.-Y. Wu, X.-H. Liu, R. Zhang, H. Liu, C.-K. Dong, J. Yang, S.A. Kulinich and X.-W. Du, *Journal of Materials Chemistry A*, 6 (2018) 9057.

64. Y. Hong, C. Li, G. Zhang, Y. Meng, B. Yin, Y. Zhao and W. Shi, *Chemical Engineering Journal*, 299 (2016) 74.

65. L. Tang, Y. Zhang, C. Li, Z. Zhou, X. Nie, Y. Chen, H. Cao, B. Liu, N. Zhang and Z. Said, *Chinese Journal of Mechanical Engineering*, 35 (2022) 1.

66. Y. He, Y. Wang, L. Zhang, B. Teng and M. Fan, *Applied Catalysis B: Environmental*, 168 (2015) 1.

67.   T. Gao, C. Li, Y. Zhang, M. Yang, D. Jia, T. Jin, Y. Hou and R. Li, *Tribology International*, 131 (2019) 51.
68.   W. He, H.-K. Kim, W.G. Wamer, D. Melka, J.H. Callahan and J.-J. Yin, *Journal of the American Chemical Society*, 136 (2014) 750.
69.   X. Wu, C. Li, Z. Zhou, X. Nie, Y. Chen, Y. Zhang, H. Cao, B. Liu, N. Zhang and Z. Said, *The International Journal of Advanced Manufacturing Technology*, 117 (2021) 2565.